Structural strain method for the fatigue evaluation of rib-deck joints with insufficient weld penetration

B. Villoria
Norwegian Public Roads Administration, Stavanger, Norway
University of Stavanger, Stavanger, Norway

ABSTRACT: The present paper studies the fatigue life of welded rib-deck (RD) joints using the equivalent structural strain approach derived from the equivalent structural stress method formalized in the ASME code. A nodal force-based framework is implemented to analyze welded RD joints with insufficient welding penetration. A purely linear elastic analysis yields overly conservative fatigue life predictions. The present paper investigates the performance of a plastic strain redistribution algorithm adapted from a method proposed by Pei (2019). A general improvement in terms of fatigue life estimation is obtained. Because of its simplicity, the Neuber's rule, already incorporated in the ASME Code, constitutes a good alternative to the discussed algorithm. The presented framework is relevant for the fatigue assessment of existing bridges with insufficient welding penetration.

1 INTRODUCTION

Orthotropic steel bridge decks (OSBDs) have been used in long-span bridges since the 1920s. However, multiple fatigue pathologies have been reported (Villoria 2021) in several typical details. The present publication focuses solely on the welded rib-deck joints of OSBDs.
It has been observed that fatigue cracks in RD welded joints (Kainuma 2018; Ocel 2017; Ya 2011) can initiate:

- from weld toe into the deck plate (Type I),
- from weld root into the deck plate (Type II),
- from the rib weld toe into the rib (Type III),
- or from the weld root into the weld itself (Type IV)

The Eurocode recommends considering bending stress in the rib as the governing stress for fatigue damage accumulation in welded RD joints. The hot spot stress is also presented as an alternative. However, in the presence of low welding penetration, these standard methods cannot capture the stress concentration at weld root that can lead to crack initiation from weld root (Types II and IV). Many alternative fatigue prediction models have been proposed but only the equivalent structural stress (Dong 2001) has been formally incorporated in ASME standards (ASME Div Code).

The present paper presents the main aspects of the equivalent structural stress approach and the associated equivalent structural strain approach, assuming initially elastic behavior. An algorithm to account for plastic redistribution is discussed and implemented to predict the fatigue life of welded RD specimens with insufficient welding penetration considering crack mechanisms Type I to IV.

Fatigue tests conducted on RD welded joints specimens with low welding penetration are described and used for validation. The accuracy of standard fatigue verification methods is evaluated and compared with the nominal and hot spot stress approaches.

2 EQUIVALENT STRUCTURAL STRAIN

2.1 *Background*

The accuracy of the equivalent structural stress (ESS) method has been documented (Dong 2005; Dong 2007) by analyzing a large amount of fatigue tests conducted on welded details. The ESS approach hinges on the linearization of the through-thickness stress along the considered crack, including the nonlinear component due to the presence of a weld notch. Dong demonstrated that for any through-thickness stress distribution, unique membrane stress σ_m and bending stress σ_b could be determined from equilibrium conditions. The elastic structural structural stress σ_s is then obtained from Equation (1). Figure 1(a) illustrates a stress distribution where the structural stress σ_s exceeds the yield stress of the material. The corrected stress is the result of strain hardening material behavior.

$$\sigma_s = \sigma_b + \sigma_m \tag{1}$$

The concept of structural strain was introduced (Dong 2014) as an extension of the structural stress concept. It is argued by Dong that the introduction of a linear strain distribution $\varepsilon_s(y)$ is consistent with the definition of the structural stress. Like the structural stress, the structural strain overcomes the challenges posed by the strain singularity at the considered weld notch. As shown in Figure 1(b), the through-thickness structural strain distribution $\varepsilon_s(y)$ can be written as the sum of a membrane ε_m and a bending $\varepsilon_b(y)$ components but also as a linear gradient as summarized in Equation (2):

$$\varepsilon_s(y) = ky + b = \varepsilon_m + \varepsilon_b(y) \tag{2}$$

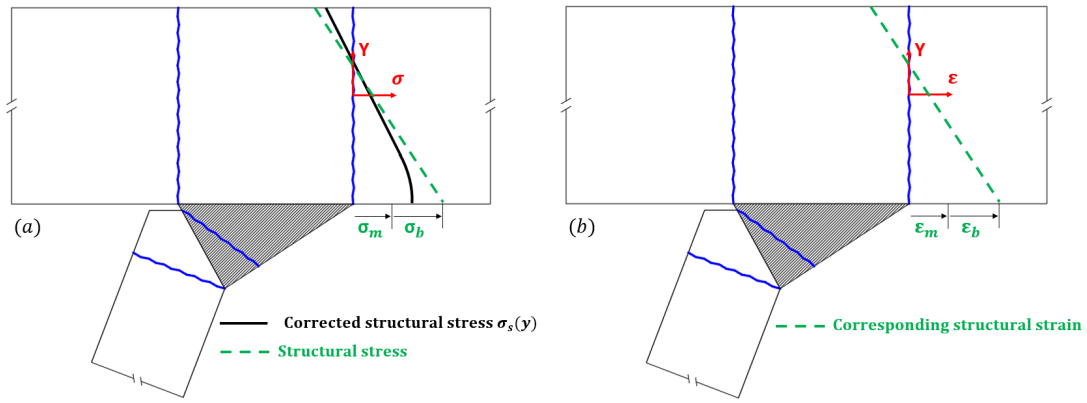

Figure 1.(a) Structural stress with nonlinear material behavior (b) Corresponding structural strain distribution.

2.2 *Nodal Force based determination of the structural stress*

A method to derive the structural stress components (Dong 2005) was implemented as part of the present work. The method requires that the nodal forces along a free-body cut at an anticipated crack plane are extracted and processed as described in the present paragraph.

Figure 2 (a) illustrates how the nodal forces components ($F_{x_{ij}}$, $F_{y_{ij}}$, $F_{z_{ij}}$) along a type I crack mechanism where the indices i and j refer to the Z- and Y-coordinates. Similar procedures are followed for the other types of crack mechanisms.

The force resultant in the X-direction at a given position i along the Z-direction is obtained by summation of the nodal forces along the Y-direction as expressed in Equation (3). Similar equations can be derived for the force resultants in the Y- and Z-direction.

$$F_{xi} = \sum_j F_{x_{ij}} \tag{3}$$

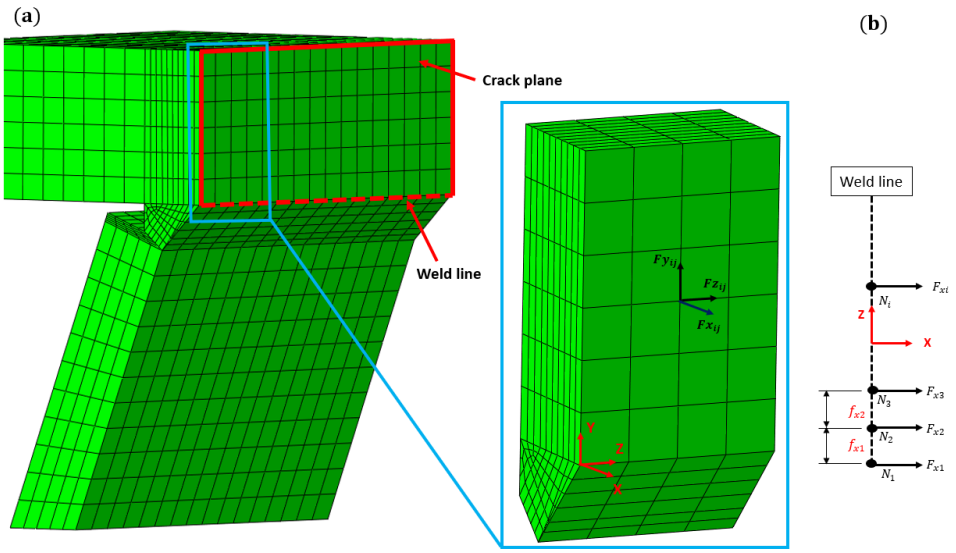

Figure 2.(a) Nodal forces along the hypothetical crack plane. (b) Line forces along the weld line

The statically equivalent line forces in the X-direction at each position *i* along the weld line (Z-direction) shown in Figure *2*.(b) are obtained from Equation (4). The equivalent line forces in the Y- and Z-direction can be obtained from a similar relation.

$$\begin{bmatrix} F_{x1} \\ F_{x2} \\ F_{x3} \\ \dots \\ \dots \\ \dots \\ \dots \\ F_{xn} \end{bmatrix} = \begin{bmatrix} \frac{l_1}{3} & \frac{l_1}{6} & 0 & 0 & \dots & 0 \\ \frac{l_1}{6} & \frac{l_1+l_2}{3} & \frac{l_2}{6} & 0 & \dots & 0 \\ 0 & \frac{l_2}{6} & \frac{l_2+l_3}{3} & \frac{l_3}{6} & \dots & 0 \\ \dots & \dots & \dots & \dots & \dots & \dots \\ \dots & \dots & \dots & \dots & \frac{l_{n-2}+l_{n-1}}{3} & \frac{l_{n-1}}{6} \\ 0 & \dots & \dots & \dots & \frac{l_n}{6} & \frac{l_{n-1}}{3} \end{bmatrix} . \begin{bmatrix} f_{x1} \\ f_{x2} \\ f_{x3} \\ \dots \\ \dots \\ \dots \\ \dots \\ f_{xn} \end{bmatrix} = \mathrm{T} \begin{bmatrix} f_{x1} \\ f_{x2} \\ f_{x3} \\ \dots \\ \dots \\ \dots \\ \dots \\ f_{xn} \end{bmatrix} \tag{4}$$

Following a similar procedure, the equivalent nodal moments (M_{xi}, M_{yi}, M_{zi}) calculated at mid-section of the free-body cut can be converted to the equivalent line moments (m_{xi}, m_{yi}, m_{zi}) by inverting the T matrix of Equation (4).

Finally, the structural stress in the X-direction at the *i-th* position along the weld line is given in Equation (5).

$$\sigma_{sx,i} = \sigma_{mx,i} + \sigma_{bx,i} = \frac{f_{x,i}}{t^2} + \frac{6\, m_{x,i}}{t^2} \tag{5}$$

2.3 *Equivalent structural strain*

The limitations of the equivalent structural stress method in the low- to medium-cycle regime were highlighted by Dong. The equivalent structural strain method was primarily formulated for the low-cycle regime to incorporate the effects of plastic redistribution.

The elastic equivalent structural strain range $\Delta\varepsilon_s^e$ can be derived from the elastic structural stress $\Delta\sigma_s^e$ by means of the Hooke's law. In presence of stresses beyond the material yield limit, ASME suggests using the Neuber's rule, expressed in Equation (6), in combination with a strain hardening law to account for plasticity redistribution to evaluate the actual stress $\Delta\sigma_s$ and strain $\Delta\varepsilon_s$ ranges.

$$\Delta\sigma_s . \Delta\varepsilon_s = \Delta\sigma_s^e . \Delta\varepsilon_s^e \tag{6}$$

ASME standards recommends the cyclic stress-strain relation given Equation (7) to model the stress-strain hysteresis loop. The parameters n_{css} and K_{css} are material dependent and can be found in appendix 3-D.7 of ASME codes.

$$\Delta\varepsilon_s = \frac{\Delta\sigma_s}{E} + 2\left(\frac{\Delta\sigma_s}{2K_{css}}\right)^{\frac{1}{n_{css}}} \tag{7}$$

Finally, an equivalent structural strain range ΔEs can be derived from Equation (8) where the parameters m, t_{ess} and $I(r)$ are defined in ASME Div Code, while the bending ratio r is defined as $r = \varepsilon_b/\varepsilon_s$.

$$\Delta E_s = \frac{\Delta\varepsilon_S}{t_{ess}^{\frac{2-m}{m}} I(r)^{\frac{1}{m}}} \tag{8}$$

A master curve was derived for the structural strain approach where the number N of cycles to failure is related to ΔEs by Equation (9). The values of C_{strain} and h_{strain} provided in Table 1 were derived from the Master E-N curves shown in (Pei 2022).

$$\Delta E_s = C_{strain-2std}.N^{-h_{strain}} \tag{9}$$

Table 1. Parameters for Master E-N curve – steel.

Statistical basis	C_{strain}	h_{strain}
Mean curve	0.09089	
Upper 68% prediction interval (mean + 2 standard deviation)	0.13633	
Lower 68% prediction interval (mean – 2 standard deviation)	0.63363	0.31950
Upper 95% prediction interval (mean + 3 standard deviation)	0.1636	
Lower 95% prediction interval (mean - 3 standard deviation)	0.05453	

3 ALGORITHM FOR PLASTIC STRAIN REDISTRIBUTION

3.1 *Stress-strain relation*

Pei suggested an altered Ramberg-Osgood relation (Pei 2019), expressed in Equation (10), allowing a clear distinction between the elastic and plastic strain components, as opposed to the original formulation by Ramberg-Osgood in which the plastic contribution is always present.

$$\begin{aligned} \varepsilon &= \frac{\sigma}{E} \quad \text{if } \sigma < \sigma_{prop} \\ \varepsilon &= \frac{\sigma}{E} + sign(\sigma) * \alpha\frac{\sigma_0}{E}\left[\left(\frac{\sigma}{\sigma_0}\right)^m - \left(\frac{\sigma_{prop}}{\sigma_0}\right)^m\right] \quad if\ \sigma \geq \sigma_{prop} \end{aligned} \tag{10}$$

The material parameters α, m, σ_0 and σ_{prop} are obtained by using a least-squares curve fitting algorithm to fit the monotonic stress-strain relation provided in Annex 3-D of Asme Div Code. The specimens considered in the present study are made of steel grade S355 for which the values α=10.5, m=12.35, σ_0=420 MPa and σ_{prop}= 295 MPa yield a satisfying fit with the monotonic stress-strain curve.

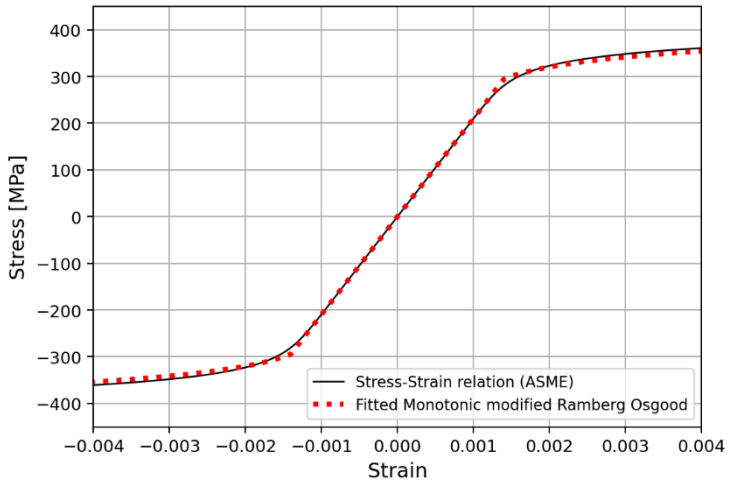

Figure 3. Modified Ramberg-Osgood stress-strain relation for steel S355

3.2 *Return mapping algorithm*

The linearized membrane σ_m and bending stresses σ_b are derived from the actual through-thickness distribution $\sigma_x(y)$ by use of the equilibrium conditions expressed in Equation (11)where *t* designates the plate thickness:

$$\sigma_m = \frac{1}{t}\int_{-t/2}^{t/2} \sigma_x(y).dy \quad \text{and} \quad \sigma_b = \frac{6}{t^2}\int_{-t/2}^{t/2} \sigma_x(y).y.dy \tag{11}$$

Using the coordinate system illustrated in Figure 1, the total strain $\varepsilon_{x,total}(y)$ can be written as the sum of a plastic component $\varepsilon_{x,p}(y)$ and an elastic component $\varepsilon_{x,e}(y)$ but also as a linear function of the vertical position y as expressed in Equation (12).

A general framework to account for nonlinear hardening effects is presented below.

$$\begin{bmatrix}\varepsilon_{x,total}(y)\\ \varepsilon_{y,total}(y)\\ \varepsilon_{z,total}(y)\end{bmatrix} = \begin{bmatrix}k_1 y + b_1\\ k_2 y + b_2\\ k_3 y + b_3\end{bmatrix} = \begin{bmatrix}\varepsilon_{x,e}(y) + \varepsilon_{x,p}(y)\\ \varepsilon_{y,e}(y) + \varepsilon_{y,p}(y)\\ \varepsilon_{z,e}(y) + \varepsilon_{z,p}(y)\end{bmatrix} \tag{12}$$

The Hooke's law allows us to write the following relation:

$$\begin{aligned}\begin{bmatrix}\sigma_x(y)\\ \sigma_y(y)\\ \sigma_z(y)\end{bmatrix} &= \begin{bmatrix}2\mu+\lambda & \lambda & \lambda\\ \lambda & 2\mu+\lambda & \lambda\\ \lambda & \lambda & 2\mu+\lambda\end{bmatrix}\begin{bmatrix}\varepsilon_{x,e}(y)\\ \varepsilon_{y,e}(y)\\ \varepsilon_{z,e}(y)\end{bmatrix}\\ &= \text{Hooke}\begin{bmatrix}\varepsilon_{x,total}(y) - \varepsilon_{x,p}(y)\\ \varepsilon_{y,total}(y) - \varepsilon_{y,p}(y)\\ \varepsilon_{z,total}(y) - \varepsilon_{z,p}(y)\end{bmatrix}\end{aligned} \tag{13}$$

After integration of the relations in Eq (11), Eq (13) can be rewritten as Equations (14) and (15):

$$\begin{bmatrix}\sigma_{m,x}(y).t\\ \sigma_{m,y}(y).t\\ \sigma_{m,z}(y).t\end{bmatrix} = Hooke\left(\begin{bmatrix}b_1\\ b_2\\ b_3\end{bmatrix}t - \begin{bmatrix}\int_{-t/2}^{t/2}\varepsilon_{x,p}(y).dy\\ \int_{-t/2}^{t/2}\varepsilon_{y,p}(y).dy\\ \int_{-t/2}^{t/2}\varepsilon_{z,p}(y).dy\end{bmatrix}\right) \tag{14}$$

$$\begin{bmatrix}\sigma_{b,x}(y).t\\ \sigma_{b,y}(y).t\\ \sigma_{b,z}(y).t\end{bmatrix} = Hooke_{mat}\left(\begin{bmatrix}k_1\\ k_2\\ k_3\end{bmatrix}.\frac{t^3}{12} - \begin{bmatrix}\int_{-t/2}^{t/2}\varepsilon_{x,p}(y).y.dy\\ \int_{-t/2}^{t/2}\varepsilon_{y,p}(y).y.dy\\ \int_{-t/2}^{t/2}\varepsilon_{z,p}(y).y.dy\end{bmatrix}\right) \tag{15}$$

The through-thickness distributions of plastic strain are initially set equal to zero. The linear gradient coefficients (k_1, k_2, k_3) and (b_1, b_2, b_3) depend on the current plastic strain tensor [$\varepsilon_{x,p}(y)$, $\varepsilon_{y,p}(y)$, $\varepsilon_{z,p}(y)$] accumulated prior to the application of the considered load step and can be determined by simple linear algebra operations from Equations (14) and (15).

The updated total strain components can now be calculated from Equation (12). Subsequently trial stresses $\left[\sigma_x^{tr}(y), \sigma_y^{tr}(y), \sigma_z^{tr}(y)\right]$ can be computed from Eq (13). The von Mises equivalent stress σ_{eq} given in Equation (16) as a function of the deviatoric stress tensor σ_{dev}.

$$\sigma_{eq} = \sqrt{\frac{3}{2}\sigma_{dev}:\sigma_{dev}} \tag{16}$$

The von Mises yield function f given by Equation (17) is expressed as a function of the trial equivalent von Mises stress and strain.

$$f^{tr}\left(\sigma_{eq}^{tr}, \varepsilon_{eq}^{p,tr}\right) = \sigma_{eq}^{tr} - \sigma_0\left[\frac{E\varepsilon_{eq}^{p,tr}}{\alpha\sigma_0} + r^m\right] \tag{17}$$

The equivalent strain $d\varepsilon_{eq}^{p}$ (Dieter 1976) is given by Equation (18) where $\overline{\varepsilon^p}$ designates the plastic strain tensor :

$$d\varepsilon_{eq}^{p} = \sqrt{\frac{2}{3}.d\overline{\varepsilon^p}:d\overline{\varepsilon^p}} \tag{18}$$

If the yield function f^{tr} given in Equation (17) becomes negative for the trial stress and strain values, then a return mapping algorithm is used to determine the equivalent stress σ_{eq} and plastic strain ε_{eq}^{p} that satisfy the so-called consistency condition imposing that the stress value is located on the yield surface. The consistency condition is expressed in Equation (19).

$$f\left(\sigma_{eq}, \varepsilon_{eq}^{p}\right) = \sigma_{eq} - \sigma_0\left[\frac{E\varepsilon_e^p}{\alpha\sigma_0} + \left(\frac{\sigma_{prop}}{\sigma_0}\right)^m\right]^{\frac{1}{m}} = 0 \tag{19}$$

Equation (20) provides a relation between the trial equivalent stress and the plastic strain increment. For the purposes of brevity, the proof of this relation is not provided in the present paper. It hinges on the plastic incompressibility of metals, further details can be found in appendix A of Pei's publication (Pei 2019).

$$\sigma_{eq} = \sigma_{eq}^{tr} - 3G\Delta\varepsilon_{eq}^{p} \tag{20}$$

Equation (19) can now be rewritten as Equation (21) by substituting σ_{eq} with the above equation.

$$f\left(\sigma_{eq}, \varepsilon_{eq}^{p}\right) = \sigma_{eq}^{tr} - 3G\Delta\varepsilon_{eq}^{p} - \sigma_0\left[\frac{E\left(\varepsilon_{eq}^{p,tr} + \Delta\varepsilon_{eq}^{p}\right)}{\alpha\sigma_0} + \left(\frac{\sigma_{prop}}{\sigma_0}\right)^{m}\right] = 0 \tag{21}$$

A numerical solver is used to obtain a plastic strain increment $\Delta\varepsilon_{eq}^{p}$ that satisfies the modified consistency condition expressed in Equation (21). The equivalent plastic strain increment $d\varepsilon_{eq}^{p}$ is normal to the yield surface f as presented in Equation (22), when associated flow rule is assumed. The scalar dλ is the scalar plastic multiplier.

$$d\varepsilon_p = d\lambda\frac{\partial f}{\partial\sigma} \tag{22}$$

The Prandtl-Reus Equations impose, for an isotropic material, proportionality between the principal plastic incremental strains $d\overline{\varepsilon_p}$ and the deviatoric stress tensor σ_{dev}, expressed in Equation (23).

$$d\overline{\varepsilon_p} = \sigma_{dev}d\lambda \tag{23}$$

By substituting $d\overline{\varepsilon_p}$ in Equation (18) and using the von Mises equivalent stress definition given in Equation (16) , the following relation for the plastic incremental strain tensor is obtained.

$$\Delta\overline{\varepsilon_p} = \frac{3}{2}\frac{\sigma_{dev}^{tr}}{\sigma_e}\Delta\varepsilon_{eq}^{p} \tag{24}$$

The updated plastic strain through-thickness distribution is given by Equation (25).

$$\begin{bmatrix}\varepsilon_{x,p}(y)\\ \varepsilon_{y,p}(y)\\ \varepsilon_{z,p}(y)\end{bmatrix}_{updated} = \begin{bmatrix}\varepsilon_{x,p}(y)\\ \varepsilon_{y,p}(y)\\ \varepsilon_{z,p}(y)\end{bmatrix}_{previous} + \frac{3}{2}\frac{\Delta\varepsilon_{eq}^{p}}{\sigma_e}\begin{bmatrix}\frac{1}{3}(2\sigma_1^{tr} - \sigma_2^{tr} - \sigma_3^{tr})\\ \frac{1}{3}(2\sigma_1^{tr} - \sigma_2^{tr} - \sigma_3^{tr})\\ \frac{1}{3}(2\sigma_1^{tr} - \sigma_2^{tr} - \sigma_3^{tr})\end{bmatrix} \tag{25}$$

The updated plastic strain distribution is then used to determine new linear strain gradient coefficients from Equations (14) and (15). New trial strain and stress distributions are then derived from Equations (12) and (13).

4 FATIGUE TEST DATA

Fatigue tests (Janss 1988) on 36 RD welded joints that were purposely designed with an insufficient penetration rate and limited edge preparation are considered for validation of the algorithm discussed in section 3. The specimens were constrained on either side of the trapezoidal stiffeners by rollers. The loads simulating the effect of traffic loading were applied unsymmetrically, therefore only the welded joints closest to the point of load application are considered. The test setup is shown in Figure 4. The dimension *p* characterizing the lack of weld penetration varies between 1.0 and 4.7 mm, while the gap *e* varies between 0.0 and 2.0 mm.

The tests aimed to explore the consequences of poor weld quality on fatigue life. They also provide a unique test series with significantly higher levels of plastic deformation than expected in typical RD joints. The test series is used to illustrate the performance of the structural strain method in presence of moderate levels of plasticity.

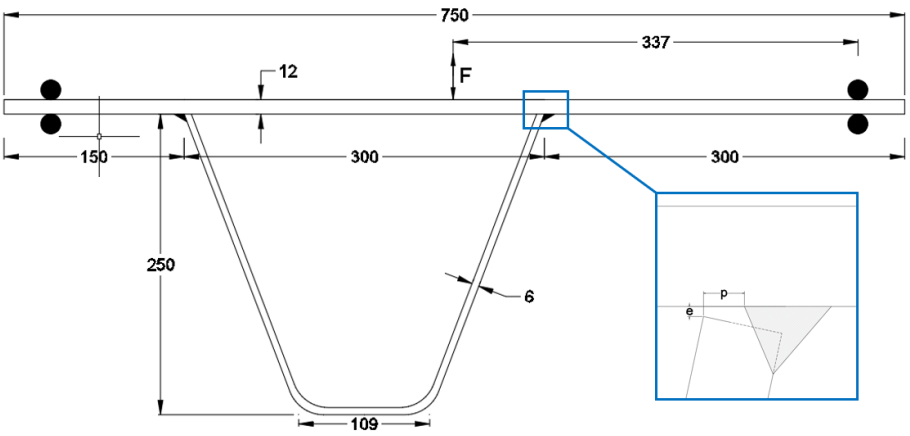

Figure 4. RD welded joint fatigue test setup and weld geometry.

5 RESULTS

5.1 *Modelling*

The general-purpose software Abaqus was used to model the different specimens. The submodelling technique was used to obtain the refined mesh required by the nodal force-based procedure described in section 2.2. Solid elements of type C3D8 are used. As shown in Figure 5, the four potential crack mechanisms expected at RD welded joints were considered in the present analysis.

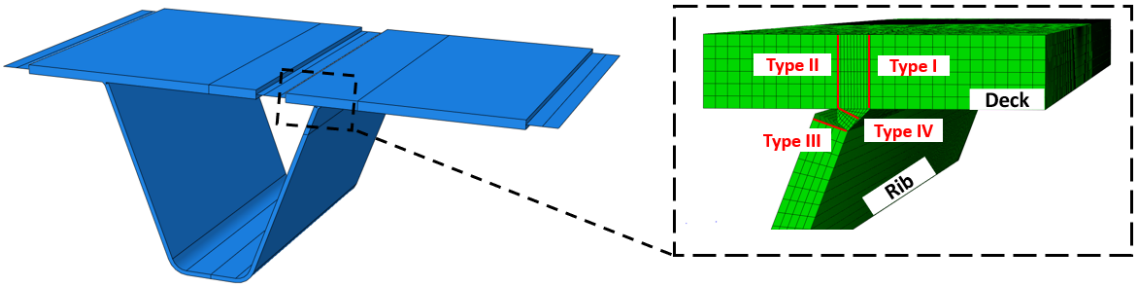

Figure 5. Abaqus model and submodel showing the four cracking mechanisms.

5.2 *Return mapping algorithm*

The return mapping algorithm described in section 3.2 was implemented to analyze the fatigue tests reported by Janss. As shown in Figure *6*, the largest strains are expected in the direction normal to the considered crack mechanism. Nonetheless, the other strain components cannot be neglected. This observation is consistent with the proposed algorithm where all three strain components are considered.

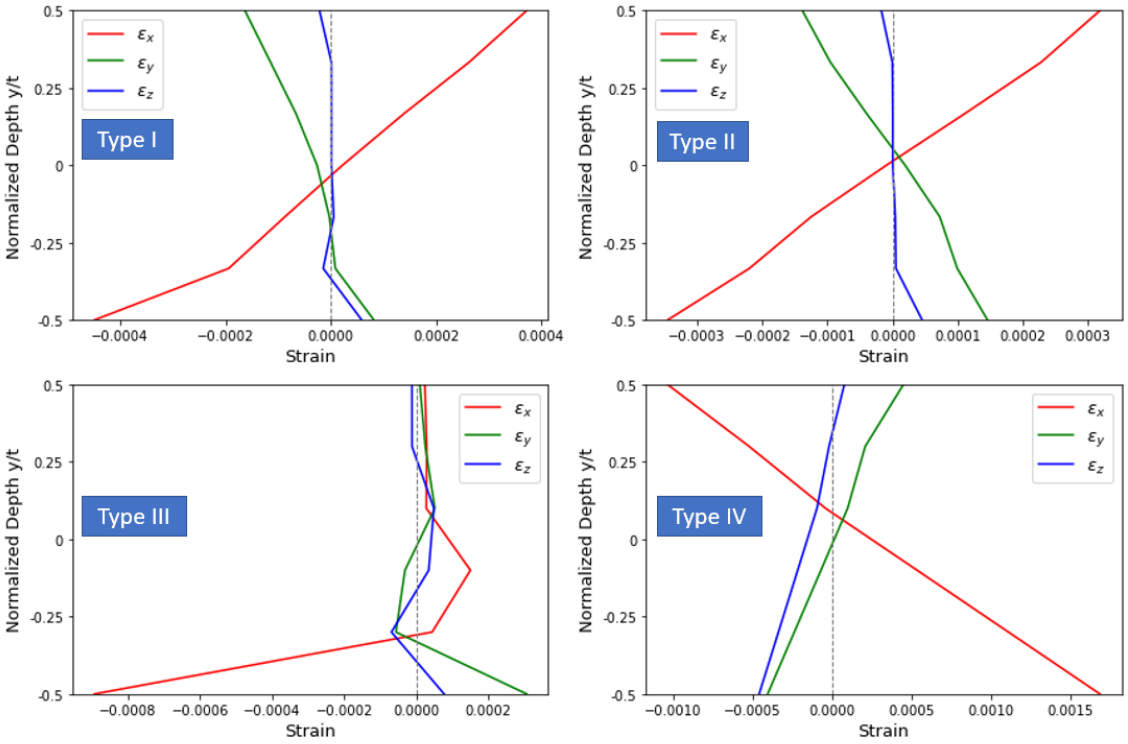

Figure 6. Strain distribution along the four crack planes for specimen-1.

The return mapping algorithm described in section 3.2, implemented in a Python script. A stable hysteresis loop forms after only one load cycle for all the specimens studied in the CRIF experiments as shown in Figure 7.

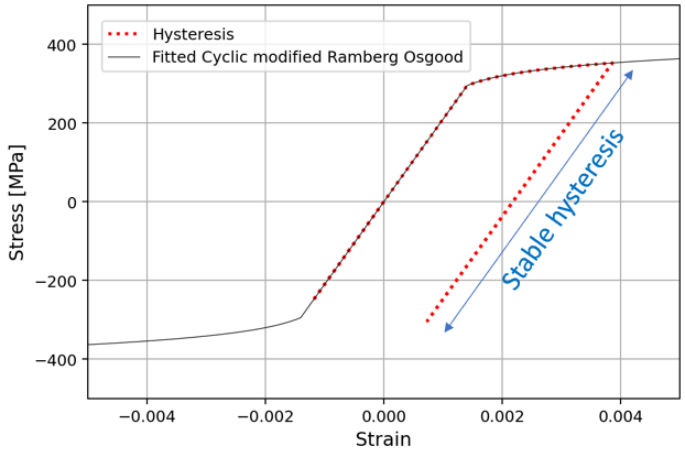

Figure 7. Formation of a stable hysteresis loop for specimen-25 of the CRIF test series

An equivalent strain range can be defined based on the Miner's linear damage accumulation rule expressed in Equation (26) where n_{cycle1} is equal to 1 and refers to the first cycle, n_{total} is the total of cycles to failure. $N_{cycle\ 1}$ and N_{rest} denote the expected number of cycles to failure corresponding respectively to the first cycle of the strain range and the stabilized strain range.

$$\frac{n_{cycle1}}{N_{cycle\ 1}} + \frac{n_{total} - n_{cycle1}}{N_{rest}} = 1 \tag{26}$$

Using Equation (9) and rearranging Equation (26), n_{total} is given in Equation (27).

$$n_{total} = 1 + \left(\frac{C_{strain}}{\Delta E_{s,rest}}\right)^{\frac{1}{h_{strain}}} \left(1 - \left(\frac{\Delta E_{s,cycle1}}{C_{strain}}\right)^{\frac{1}{h_{strain}}}\right) \quad (27)$$

The equivalent structural strain range $\Delta E_{s,eq}$ is then obtained by Equation (28).

$$\Delta E_{s,eq} = C_{strain} {n_{total}}^{-h_{strain}} \quad (28)$$

5.3 *Neuber's rule*

The ASME Code suggests that the Neuber's rule given in Equation (6) can be used to correct the elastic stress obtained from a linear elastic analysis. As illustrated in Figure 8, the corrected stress is obtained by determining the intersection between the Neuber's curve passing by the elastic stress and the considered stress-strain curve. The modified Ramberg Osgood curve described in section 3.1 is here used as stress-strain curve.

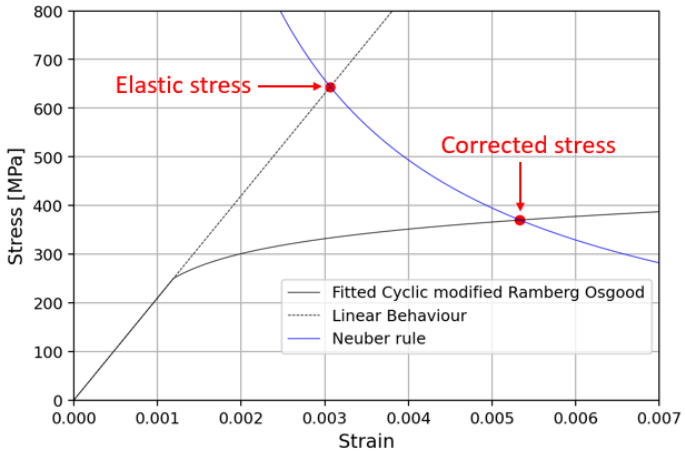

Figure 8. Stress correction by Neuber's rule (ASME) – specimen 25 from CRIF series.

5.4 *Standard methods*

As shown in Figure 9, the nominal stress and hot spot stress methods yield nonconservative fatigue life predictions. The nominal stress in RD welded joints is defined as the bending stress in the rib (Eurocode) which entails that the method overlooks the stress concentration at the weld root resulting from insufficient penetration. Similarly, the hot spot stress is determined through a stress extrapolation procedure along the deck and rib surfaces, leading to the same conclusion.

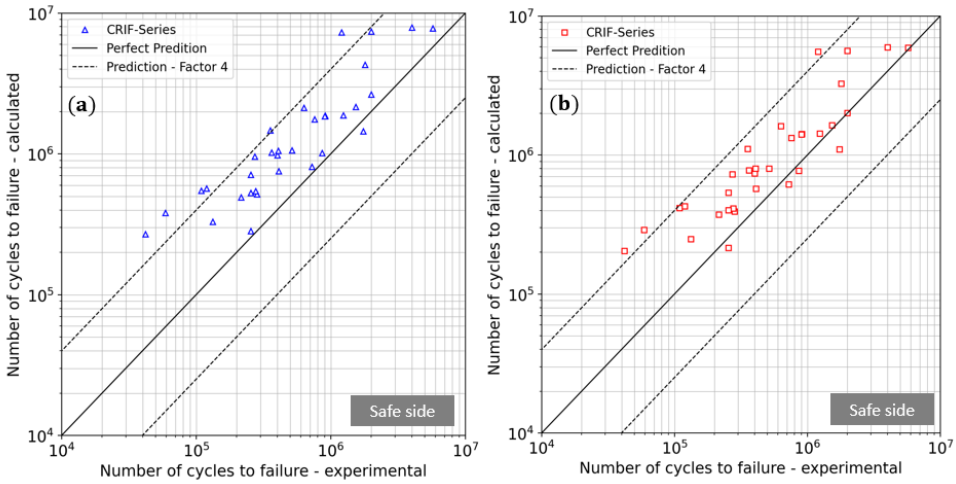

Figure 9. Experimental fatigue lives versus fatigue lives calculated by (a) nominal stress (b) Hot spot approach.

5.5 *Comparison and discussion*

As shown on Figure 10 (a and b), the proposed strain hardening algorithm (corresponding to the points labelled R-O Strain Hardening) yields a better fatigue prediction than the initial linear ESE approach. The performance of the Neuber's rule is satisfactory even though it gives generally more conservative fatigue life estimations than the return mapping algorithm.

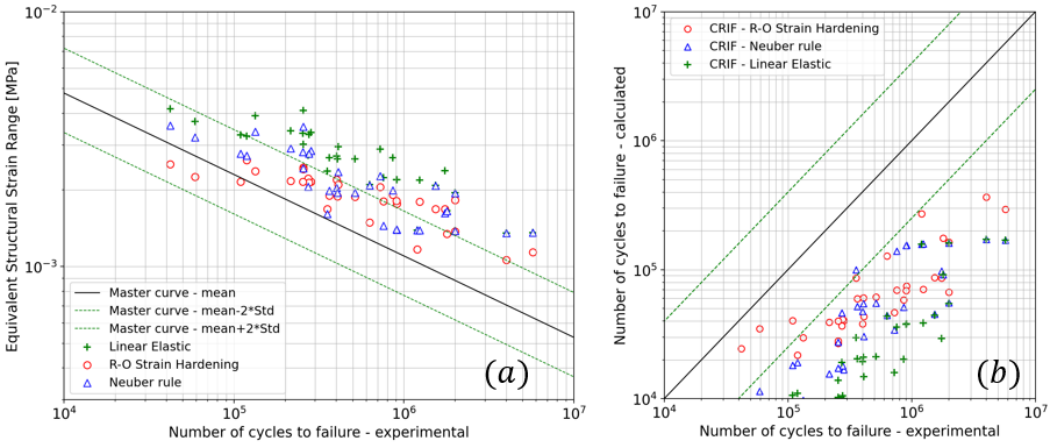

Figure 10. (a) ESE ranges from linear elastic approach, nonlinear strain-hardening algorithm and Neuber's rule (b) Expected number of cycles to failure

The relative error index, for the linear ESE method and the discussed algorithm to account for strain hardening effects, is calculated as defined in Equation (29) where $N_{experimental}$ is the experimental number of cycles to failure and $N_{calculated}$ is the number of cycles to failure calculated by the considered method.

$$\mathrm{I} = \frac{N_{experimental} - N_{calculated}}{N_{experimental}} \cdot 100 \tag{29}$$

The histogram of the frequency count of the relative error index between the calculated and experimental fatigue lives is shown for both methods in Figure 11 where the improved fatigue life prediction by the discussed strain hardening algorithm is noticeable.

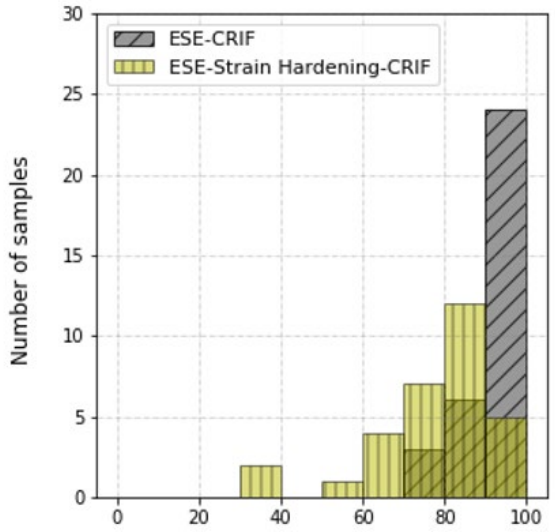

Figure 11. Error index – Comparison of predicted and experimental lives.

Figure 9 shows that the nominal stress and hot spot stress approaches lead to nonconservative fatigue life predictions. The ESE method, assuming purely linear behavior, yields only conservative fatigue life predictions. The algorithm, described in section 3, to incorporate strain hardening effects for the ESE approach, provides notably improved fatigue life predictions. Implementing Neuber's rule in combination with a cyclic stress-strain curve, as suggested by ASME Div Code improves fatigue life predictions in comparison with the linear analysis but displays a lower level of performance than the discussed algorithm.

6 CONCLUSIONS

The present paper presents a framework for the evaluation of rib-deck (RD) welded joints with insufficient weld penetration. The method hinges on the concept of equivalent structural strain in a nodal force-based formulation. By incorporating the effect of plastic strain redistribution, the algorithm provides more accurate fatigue life predictions than standard methods, addressing the limitations of purely elastic analyses which tend to be overly conservative.

Fatigue tests on RD welded joints with insufficient weld penetration are used to validate the accuracy of the algorithm. The use of the Neuber's rule, as recommended by ASME standards, offers a simpler yet effective alternative although it gives more conservative fatigue life estimations.

This study suggests that the equivalent structural strain method, combined with an algorithm for plastic strain redistribution, can constitute a valuable tool for assessing the fatigue life of existing bridges where low weld penetration might be a concern.

REFERENCES

Boiler, A. S. M. E., & Code, P. V. (2007). Sec VIII, Div. 2 (ASME BPVC-VIII-2 e2007). *New York, NY:American Society of Mechanical Engineers*.

Dieter, G. E., & Bacon, D. 1976. Mechanical metallurgy (Vol. 3, pp. 43-53). New York: McGraw-hill.

Dong, P. 2001. *A structural stress definition and numerical implementation for fatigue analysis of welded joints*. International journal of fatigue, 23(10), 865-876.

Dong, P. 2005. *A robust structural stress method for fatigue analysis of offshore/marine structures*. J. Offshore Mech. Arct. Eng., 127(1), 68-74.

Dong, P., Hong, J. K., & De Jesus, A. M. 2007. *Analysis of recent fatigue data using the structural stress procedure* in ASME Div 2 rewrite.

Dong, P., Pei, X., Xing, S., & Kim, M. H. 2014. *A structural strain method for low-cycle fatigue evaluation of welded components*. International Journal of Pressure Vessels and Piping, 119, 39-51.

Eurocode 3: *Design of Steel Structures - Part 1-9: Fatigue: 2010*, European committee for Standardization: Brussels.

Janss, J. (1988). *Fatigue of welds in orthotropic bridge deck panels with trapezoidal stiffeners*. Journal of Constructional Steel Research, 9(2), 147-154.

Kainuma, S., Yang, M., Jeong, Y. S., Inokuchi, S., Kawabata, A., & Uchida, D. 2018. *Fatigue behavior investigation and stress analysis for rib-to-deck welded joints in orthotropic steel decks*. International Journal of Steel Structures, 18, 512-527.

Ocel, J. M., Cross, B., Wright, W. J., & Yuan, H. 2017. *Optimization of rib-to-deck welds for steel orthotropic bridge decks* (No. FHWA-HRT-17-020). United States. Federal Highway Administration.

Pei, X., & Dong, P. 2019. *An analytically formulated structural strain method for fatigue evaluation of welded components incorporating nonlinear hardening effects*. Fatigue & Fracture of Engineering Materials & Structures, 42(1), 239-255.

Pei, X., Li, X., Zhao, S., Dong, P., Liu, X., & Xie, M. 2022. Low cycle fatigue evaluation of welded structures with arbitrary stress-strain curve considering stress triaxiality effect. International Journal of Fatigue, 162, 106969.

Villoria, B., Siriwardane, S. C., & Lemu, H. G. 2021. Review on fatigue life assessment methods for welded joints in orthotropic steel decks of long-span bridges. In *IOP Conference Series: Materials Science and Engineering* (Vol. 1201, No. 1, p. 012036). IOP Publishing.

Ya, S., Yamada, K., & Ishikawa, T. 2011. *Fatigue evaluation of rib-to-deck welded joints of orthotropic steel bridge deck*. Journal of Bridge Engineering, 16(4), 492-499.